Measurement of the $n=2$ density operator for hydrogen atoms produced by passing protons through thin carbon targets*

Gerald Gabrielse†
Department of Physics, University of Chicago, Chicago, Illinois 60637
and Argonne National Laboratory, Argonne, Illinois 60439
(Received 22 May 1979; revised manuscript received 23 April 1980)

Measurements of the $n=2$ density operator and the probability for $n=2$ production are reported for hydrogen atoms produced by passing 20 to 1000 keV protons through thin carbon targets. Measurements of the dependence of $2p$ production on the number of protons in the incident projectile and on the time this proton cluster spends within the foil are also discussed.

I. INTRODUCTION

During the past ten years, beam-foil spectroscopy has produced a great deal of information about many atoms and ions.[1] At the same time, there have been several studies of the ion-target interaction itself.[2] These interaction studies, mainly of charged-state and excited-state populations, were initially motivated by the hope that a better understanding of the beam-foil light source would enhance its use as a spectroscopic tool. The interaction studies discussed in this paper are measurements of components of the density operator for atomic hydrogen produced by sending protons through thin carbon targets. Related interaction studies, which will not be discussed here, include measurement of the alignment and orientation of nonhydrogenic atoms and ions as they move downbeam from a thin target, which may be oriented at any angle with respect to the beam,[1] measurements of the secondary electrons driven from thin targets by the projectile beam,[3] and the energy-loss measurements which reveal a "Coulomb explosion" of molecular beams.[4] The recent review of Berry[1] together with the references cited cover these topics.

Hydrogen atoms are particularly convenient projectiles to use in studying the interaction of an ion beam and a target, because the hydrogen wave functions are well known and hence do not complicate the interaction study. Accordingly, measurements are reported of the $n=2$ density operator for hydrogen atoms produced by passing 20 to 1000 keV protons through thin carbon targets normal to the proton beam. Owing to the axial symmetry of the interaction, the $n=2$ density operator is completely specified by only five observables. Of these, only the alignment has been previously measured over an appreciable energy range, first by Dobberstein, Andrä, Wittman, and Bukow[5] and, more recently, by Winter and Bukow.[6] The interference beat measurements described in Sec. II make it possible to extract the remaining four observables, each of them being normalized to the probability that when a neutral hydrogen atom is produced it is produced in a $n=2$ state. The analysis required to extract these observables from Ly α decay curves is discussed in Sec. III. The measured density operator is discussed in Sec. IV and is compared to the measurement by Alguard and Drake[7] of the relative populations of hydrogen $2s$ and $2p$ states at several incident proton energies and to the measurement by Gaupp, Andrä, and Macek[8] of the relative phase of the $2s$ and $2p$ excitation amplitudes at several incident proton energies. This last measurement was reported shortly after the initial work by Sellin, Moak, Griffin, and Biggerstaff,[9] who followed a suggestion made by Eck.[10] Measurements of the probability for excitation of $n=2$ states are reported in Sec. V.

We analyze our measurement using the notation suggested by Gabrielse[11] as a generalization of Fano and Macek's approach to include hydrogenic states and strong fields. This notation cleanly distinguishes three stages in the time-resolved measurement: a hydrogen formation process completed by $t=0$, a time evolution between $t=0$ and $t=t$ in the presence of a strong electric field, and a measurement of the unpolarized component of the Ly α radiation at $t=t$. Because we use a Hermitian unit tensor base, we work with observables directly and are able to make full use of both spatial and time-reversal symmetries of each stage. In particular, we are able to use time-reversal symmetry to provide a qualitative discussion of the way in which each observable at $t=0$ contributes to subsequent Ly α radiation, before explicit numerical calculation of these functions.

Three of the five observables we use to analyze our time-resolved measurement are proportional to the real or imaginary part of a density matrix element in standard bases. Two are linear com-

TABLE I. The observables $\langle (nL)(nL)^{\dagger}; kq\epsilon p \mid \rho \rangle$ in the notation of Ref. 11. The quantum numbers k, q, ϵ, and p are the tensor rank, the magnitude of the tensor component, the eigenvalue for rotations of π about the $\hat{y}$ axis, and the time-reversal eigenvalue. R and I denote real and imaginary parts.

Observables	In $i^L Y_{LM}$ base	In Y_{LM} base
$\langle (2s)(2s)^{\dagger}; 0011 \mid \rho \rangle$	ρ_{2s}	Same
$\langle (2p)(2p)^{\dagger}; 0011 \mid \rho \rangle$	$3^{-1/2}(\rho^R_{2p0} + 2\rho^R_{2p1})$	Same
$\langle (2p)(2p)^{\dagger}; 2011 \mid \rho \rangle$	$(\frac{2}{3})^{-1/2}(\rho^R_{2p1} - \rho^R_{2p0})$	Same
$\langle (2s)(2p)^{\dagger}; 10\text{-}11 \mid \rho \rangle$	$-\sqrt{2}\rho^I_{2sp0}$	$-\sqrt{2}\sigma^R_{2sp0}$
$\langle (2s)(2p)^{\dagger}; 10\text{-}1\text{-}1 \mid \rho \rangle$	$-\sqrt{2}\rho^R_{2sp0}$	$\sqrt{2}\sigma^I_{2sp0}$

binations of the remaining two density matrix elements. Table I allows easy conversion. Our results are plotted as the real and imaginary parts of density matrix elements. We do this because one of the two density matrix elements which are not proportional to a single observable, is nearly constant with respect to energy over the range measured. Further discussion of the measured $n=2$ density operator is necessarily brief and phenomenological because no convincing model is presently available. The only model available at all is the "surface electric field model" suggested by Eck[12] and then generalized by Lombardi.[13] This model has been recently used by Kupfer and Winter[14] to interpret the earlier hydrogen data; however, it seems to be applied incorrectly to the earlier experimental data. We find this model to be impossible to test by existing data when correctly applied.

If instead of protons we send H_2^+ or H_3^+ molecules through thin carbon targets, the protons from a single molecule remain correlated inside the foil. The effects of this correlation upon the energy lost by each proton and upon its trajectory is well known in the Coulomb explosion literature.[4] Gaillard, Poizat, Ratkowski, Remillieux, and Auzas[15] reported a study of the effects of such correlation upon the number of neutral hydrogen atoms produced per incident proton, as a function of the time spent by the protons within the foil. In Sec. VI we report similar studies of $2p$ production, made by measuring the Ly α radiation intensity per incident proton, as a function of foil thickness. The long-dwell-time effects we observe permit a simple interpretation.

II. THE INTERFERENCE BEAT MEASUREMENTS

The apparatus used to measure Ly α interference beats is drawn to scale in Fig. 1. Beams of

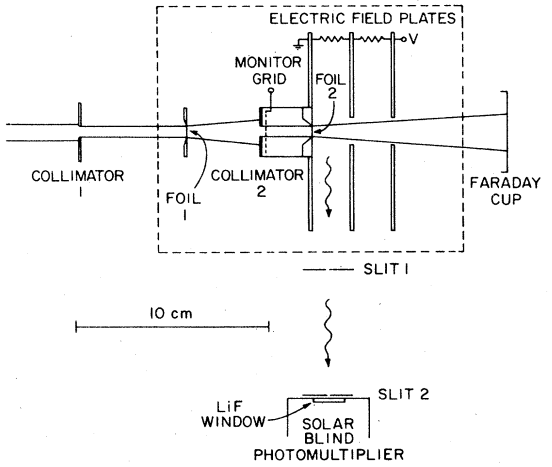

FIG. 1. The apparatus.

H^+, H_2^+, or H_3^+, selected by a bending magnet, enter this apparatus from the left. We obtained H^+ and H_2^+ beams of kinetic energy from 20 to 120 keV from a small accelerator constructed and located at Argonne National Laboratory. We obtained 330- to 2000-keV beams of H_2^+ and H_3^+ from the Argonne Dynamitron accelerator. The beam was collimated at the front of our target chamber by the $\frac{1}{4}$-in.-diameter collimator 1.

To produce proton beams at the higher energies, we dissociated H_2^+ and H_3^+ beams in foil 1 via the Coulomb explosion mechanism. The lower-energy measurements we made using proton beams with foil 1 removed. We observed no molecular effects when the dissociation foil was in place. The higher-energy measurements, made with incident H_2^+ and H_3^+ beams of the same velocity, were consistent with each other within experimental uncertainties in all cases and agreed with the proton results in the 110-keV region, where the proton beam was used and foil 1 was removed. The dissociated beam was collimated by the $\frac{3}{16}$-in. collimator 2, passed through a grid used to monitor the beam current, and then entered foil 2, which was $\frac{1}{4}$ in. in diameter. The grid sampled only the beam which would pass through the second foil, since collimator 2 was smaller than foil 2. The alignment of collimators and foils was verified by a darkened grid pattern which could be seen centered on foil 2 when it was held up to a light following a run.

The second foil was mounted upon a stainless steel field plate which measured 4 in. by 2 in. and was machined to a tolerance of 0.002 in. Two similar $\frac{1}{8}$-in. stainless plates, containing $\frac{5}{8}$-in. holes to pass the beam, were mounted downbeam from the foil plate using $\frac{3}{4}$-in.-long plexiglass spacers located near the four corners of the

plates. The foil plate was grounded and a voltage was applied to the second and third plates via two identical resistors, both of which were thermally coupled out of the vacuum chamber. The sole purpose of the third plate was to minimize the fringing field due to the hole in the second plate. We were able to reverse kilovolt potentials with a time constant of microseconds. A digital voltmeter continuously monitored the potential difference between the foil plate and plate 2. We used electric fields of 140 and 250 V/cm. The measured excitation parameters discussed in Sec. IV were not dependent upon the electric field magnitude within our uncertainties.

Excited neutral hydrogen atoms, produced as a result of the proton-target interaction, decayed as they traveled downbeam in the constant electric field. We measured the intensity of Ly α photons emitted perpendicular to the beam axis, between the foil plate and field plate 2. More precisely, we measured the number of Ly α photons which passed through two vertical slits, as diagrammed. The slit height of $\frac{1}{2}$ in. allowed us to see a complete vertical slice of the beam. A slit width of 0.5 mm resulted in a spatial resolution trapezoid with full width at half maximum (FWHM) of about 0.6 mm, as measured by passing a very narrow slit between the beam and the detector [inset to Fig. 2(a)]. We chose this slit width to allow a usable count rate and so that the high-frequency fine-structure interference oscillations would be averaged out, leaving only the Lamb-shift interference oscillations as modified by the electric field. An EMR photomultiplier (model 541F-08-18) with a cesium-telluride photocathode detected the 1215 Å Ly α photons with a quantum efficiency of about 5%. The tube sensitivity drops off dramatically above 3000 Å, and a lithium-fluoride window transmits only above 1050 Å. As a result the only hydrogen transition detected was Ly α. We did observe carbon emission due to carbon target ions, but only when our spatial resolution allowed the photomultiplier to look directly at the foil. Our Ly α detection system was not sensitive to the polarization of the radiation and did not detect appreciable residual gas excitation of the hydrogen beam at pressures of about 10^{-6} Torr maintained within our target chamber.

All of the apparatus located within the dotted rectangle in Fig. 1 was mounted upon four linear bearings which rode two $\frac{3}{8}$-in.-diameter rods. This whole assembly could thus be moved up- and downbeam using a $\frac{3}{8}$-32 screw with a reproducibility measured to be better than 0.04 mm. The screw in turn was rotated by a stepping motor which was controlled by a PDP-11 minicomputer. The PDP-11 also switched the kilovolt potential

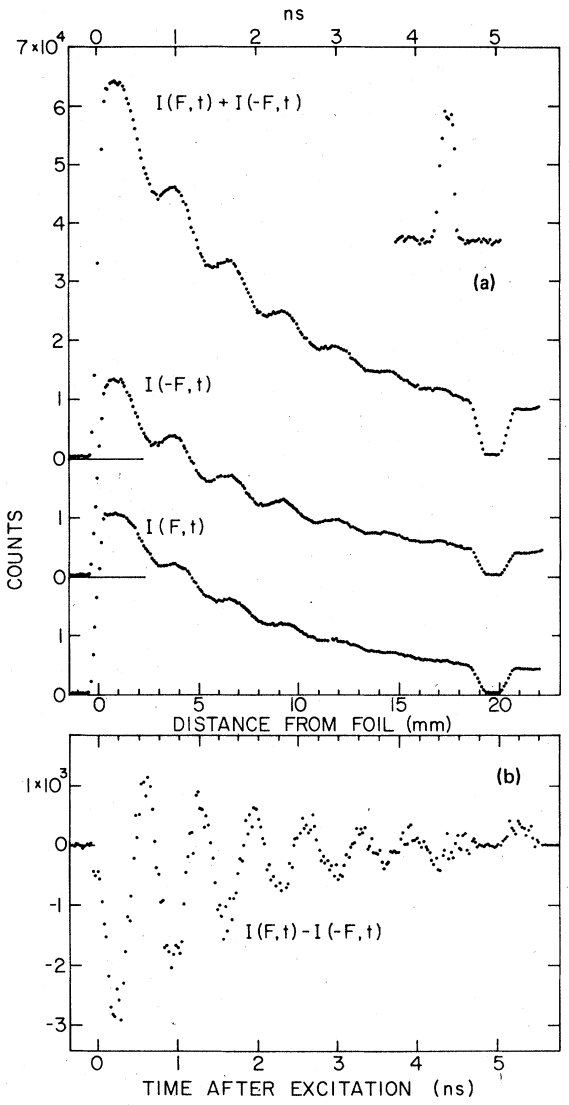

FIG. 2. Unpolarized Ly α radiation intensity as a function of distance and time from the foil surface as observed during a measurement.

applied to the electric field plates via high-voltage relays. A Ly α intensity measurement was made with an electric field parallel, $I(F,t)$, and antiparallel, $I(-F,t)$, to the beam direction. The field plate assembly was then stepped upbeam by approximately 0.11 mm and the Ly α intensity measurements were repeated. Both $I(F,t)$ and $I(-F,t)$ were displayed on a Tektronics terminal during the run, as were $I(F,t)+I(-F,t)$ and $I(F,t)-I(-F,t)$, allowing close monitoring of the run. A typical example of these four curves is given in Fig. 2 for a proton energy of 106 keV and an electric field strength of 250 V/cm. The steep rise on the left of the figure corresponds to the

foil coming into view of the detector. The shadowing of the beam by electric field plate 2 is clearly visible on the right. The time per channel was also accumulated and was displayed from time to time to check the normalization and the stability of the beam.

Extracting the $t=0$ density operator from the Ly α intensity measurements required knowing the position of foil 2 as accurately as possible. We could easily measure the position of the field plate upon which foil 2 was mounted to 0.05 mm. Despite the sharp edge on the aperture covered by the foil, however, we found that the self-supporting foil often sagged inside this aperture by as much as 0.1 mm, making it desirable to determine the foil position from the Ly α intensity measurements. We measured the movement of the foil caused by the ion beam and the electric fields we applied by reflecting a laser beam from the foil's surface onto a screen. We found that reversing our electric fields changed the foil position by less than 0.04 mm (about 0.4 of a channel). The ion beam moved the foil surface downbeam from the beam-off position by less than 0.16 mm. Although this limit is nearly two channels, we measured the foil position automatically during every run, and hence were able to correct for small beam-induced displacements.

III. ANALYSIS OF THE MEASUREMENT

The protons used in this experiment had velocities of 2–12 mm/ns (approximately 1–6 atomic units) and traveled through carbon targets which were approximately 5 $\mu g\,cm^2$ thick (about 600 atomic units). The proton-foil interaction thus lasted approximately 5×10^{-15} sec (200 atomic units). We detected Ly α photons emitted by hydrogen atoms in $n=2$ states as a function of the distance they had traveled from the target. Our spatial resolution translated into a time resolution of approximately 2×10^{-10} sec (10^7 atomic units). Measured against our detection time scale, the proton-target interaction thus occurred instantaneously, at a time we call $t=0$. We assume that the proton-target interaction is independent of nuclear and electronic spin, and hence that the $t=0$ density operator (like the incident beam) is unpolarized with respect to these spins.

Because the beam-target interaction is axially symmetric about the beam axis ($\hat{z}$), the $n=2$ density operator at $t=0$ is specified by only five parameters. For our analysis of the time-resolved measurement we choose to use five of the orbital observables suggested and discussed by Gabrielse.[11] These are listed in Table I along with equivalent expressions in standard bases. By using these orbital observables we can directly take advantage of time-reversal symmetry, as well as spatial symmetry, to describe qualitatively the contribution of each observable to to subsequent electric-dipole radiation.

The unpolarized component, $I(F,t)$, of the Ly α radiation emitted in the $\hat{y}$ direction by an $n=2$ hydrogen atom traveling through a constant electric field $\vec{F}=F\hat{z}$ can be expressed as a sum over the five nonzero $t=0$ density-operator components listed in Table I (using the notation of Ref. 11):

$$I(F,t)=\sum\langle D(E1,E1)|\,U(F,t)\,|(nL)(\tilde{n}\tilde{L})^{\dagger};kq\epsilon p\rangle \times\langle(nL)(\tilde{n}\tilde{L})^{\dagger};kq\epsilon p|\,\rho(0)\rangle\,. \tag{1}$$

The time-dependent coefficients contain the detection operator for electric-dipole radiation, $D(E1,E1)$, and the time-evolution operator $U(F,t)$ which contains all the dependence upon time t and the electric field F. Because only the $2p$ states decay via $E1$ radiation and because we observe only the unpolarized component of the light traveling in the $\hat{y}$ direction, the time-dependent coefficients can be written as

$$\langle D(E1,E1)|U(F,t)|(nL)(\tilde{n}\tilde{L})^{\dagger};kq\epsilon p\rangle = \sum_{k'=0,2}\langle D(E1,E1)|(2p)(2p)^{\dagger};k'011\rangle\langle(2p)(2p)^{\dagger};k'011|\,U(F,t)\,|(nL)(\tilde{n}\tilde{L})^{\dagger};kq\epsilon p\rangle\,. \tag{2}$$

The first factor on the right is a component of the detection operator for electric-dipole radiation. It can be simply evaluated using the expressions provided in Ref. 11. The second factor is a component of the time-evolution operator and can only be calculated numerically for a hydrogen atom decaying in the presence of an electric field. Its properties, as discussed in Ref. 11, are used in the following paragraphs to discuss the major features of the five time-dependent coefficients.

The time dependence of the coefficients is classified by the time-reversal quantum numbers (p and p') which label the evolution-operator components[11] in Eq. (2). The coefficients which correspond to the four time-reverse even components of the $t=0$ density operator (those with

$p = 1$) contain components of the evolution operator,

$$\langle (2p)(2p)^\dagger; k'01p' | U(F,t) | (nL)(\tilde{n}\tilde{L})^\dagger; kq\epsilon p \rangle ,$$

for which $p = p'$. Such oscillatory components vary approximately as $\cos(\omega t)$, where ω is the angular Lamb-shift frequency as modified by the electric field. These oscillatory terms are superimposed upon decaying exponential terms which may be regarded as cosine oscillations with zero frequency. In addition there are terms which are smaller by the ratio of the $2p$-decay width over the Lamb-shift angular frequency. These terms are due to the inclusion of decay in a Wigner-Weisskopf approximation. The time-dependent coefficient corresponding to the time-reverse odd component of the $t = 0$ density operator ($p = -1$) includes a time-evolution operator for which $p' = -p$ and, as a result, the time-dependent coefficient varies as $\sin(\omega t)$, except for the small decay-induced violations. The nonoscillatory exponential term is also very small since the leading terms vanish, being sines of zero frequency.

Changing the direction of the external electric field is equivalent to a parity transformation of the atomic evolution operator.[11] As a result, the even- or odd-parity components of the $t = 0$ density operator correspond to time-dependent coefficients which are even or odd in the electric field, respectively. The sum $I(F,t) + I(-F,t)$, illustrated in Fig. 2(a), is thus linear in the three even-parity components of the $t = 0$ density operator. The difference $I(F,t) - I(F,t)$, illustrated in Fig. 2(b), is linear in the two odd-parity components. Eck first noticed this dependence upon the sign of the field in two-state approximations of time-dependent coefficients,[10] and Lombardi, Giroud, and Macek related the dependence upon field direction to the parity of the $t = 0$ density matrix element.[16]

The detector's time resolution was chosen to average out the fine-structure oscillations in the Ly α decay curves. As a result, we observe only the lower-frequency oscillations which correspond to the Lamb shift, as modified by the electric field. An important consequence of this averaging is that the time-dependent coefficients

$$\langle D | U | (2p)(2p)^\dagger; 0011 \rangle \text{ and } \langle D | U | (2p)(2p)^\dagger; 2011 \rangle$$

are nearly proportional to each other, making it very difficult to extract both of the associated $t = 0$ density-operator components from our measurements. In our data analysis we therefore used the ratio of these components as measured by Winter and Bukow,[6] who used a reflection polarimeter to measure the polarization of Ly α radiation emitted by foil-produced hydrogen atoms in a field-free region.

The numerical calculation of the time-dependent coefficients is straight forward but laborious. We evaluate these coefficients exactly in the two parts suggested in Eq. (2). The detection-operator components

$$\langle D(E1, E1) | (2p)(2p)^\dagger; k'011 \rangle$$

are evaluated using expressions provided in Ref. 11. The evolution-operator components

$$\langle (2p)(2p)^\dagger; k'011 | U(F,t) | (nL)(\tilde{n}\tilde{L})^\dagger; kq\epsilon p \rangle$$

are evaluated numerically and include all fine and hyperfine structures. First, we diagonalize the non-Hermitian Hamiltonian $\tilde{H}$ which governs the post-interaction time development of the hydrogen atom. Each diagonal matrix element

$$(nLSJIFM | \tilde{H} | nLSJIFM)$$

is the sum of an energy and a total decay width multiplied by $-\frac{1}{2}i$. The off-diagonal matrix elements of $\tilde{H}$ are the field coupling terms

$$(nLSJIFM | zF | n\tilde{L}\tilde{S}J\tilde{I}\tilde{F}\tilde{M}) ,$$

where F is the applied electric field. The eigenvalues and eigenvectors of $\tilde{H}$ are used to obtain the evolution-operator components in terms of the coupled basis. Because the $t = 0$ density operator is unpolarized with respect to nuclear and electronic spins, a sum over these coupled components yields the time-evolution-operator components desired.

We made nonlinear least-squares fits of the Ly α decay curves to Eq. (1) using the exact coefficients

$$\langle D(E1, E1) | U(F,t) | (nL)(\tilde{n}\tilde{L})^\dagger; kq\epsilon p \rangle$$

discussed above, modified to account for the measured spatial resolution trapezoid [inset to Fig. 2(a)]. The sum curve is first fit to the three even-parity terms of Eq. (1) with the ratio of

$$\langle (2p)(2p)^\dagger; 0011 | \rho(0) \rangle \text{ and } \langle (2p)(2p)^\dagger; 2011 | \rho(0) \rangle$$

constrained to be the ratio measured by Winter and Bukow.[6] The ratio of

$$\langle (2s)(2s)^\dagger; 0011 | \rho(0) \rangle \text{ to } \langle (2p)(2p)^\dagger; 0011 | \rho(0) \rangle$$

we thus obtain depends primarily upon the amplitude of the interference beat and is insensitive to variations in the ratio obtained from Ref. 6 given by the uncertainties of Ref. 6. We also extract the velocity of the hydrogen atom and the position of the foil from the sum fit.

The velocity and foil position are functions primarily of the interference beat frequency and phase, respectively. We next fit the difference

curve to the two odd-parity terms of Eq. (1) using the foil position determined from the sum fit. We thus obtain the ratio of the odd-parity-density-operator components and their ratios to the density-operator components extracted from the sum fit. We account for cascading into the $n=2$ states by including an extra exponential term in both the sum and difference fits. The lifetime of this extra term is constrained to be the average lifetime for the $n=3$ states in the appropriate electric field. Numerical experiments indicated that this procedure was adequate, provided that the decay curve was measured over at least several Lamb-shift periods. At the higher proton energies we measured fewer Lamb-shift periods and were unable to correct for the cascade contributions as well as at the lower energies. A better accounting for cascade contributions would only be possible if the initial $n=3$ sublevel populations were known. In all cases the cascade contributions determined from the fitting were comparable in magnitude to that measured by Bukow, *et al.*[17]

IV. THE MEASURED DENSITY OPERATOR

Three of the five observables we use to analyze the time-resolved measurement are proportional to the real or imaginary part of a single density matrix element in the standard bases (see Table I). The first (a scalar) is the relative probability for producing a $2s$ state or, equivalently, the $2s$ contribution to an electric-monopole moment. The fourth is the average value of a component of a vector which is even under time reversal, and thus is an electric-dipole moment. The fifth is different only in that it is odd under time reversal but is much less familiar. It has been previously interpreted as the average value of the linear momentum of the electron $\langle\vec{p}\rangle$.[10] We prefer $\langle\vec{r}\times\vec{L}\rangle$, suitably symmetrized, since $\langle\vec{p}\rangle$ vanishes identically for a pure hydrogenic state. Alternatively, this fifth observable is proportional to $\langle r^{-2}r\times L\rangle$, suitably symmetrized, the tangential component of the linear momentum.[11]

The second and third observables are very familiar even though proportional to a linear combination of density-operator components in the standard base. The second is the probability of $2p$ production or, alternatively, the contribution of $2p$ to the electric-monopole moment, i.e., the fraction of the electron charge in $2p$. The third observable has rank 2 and is proportional to the average value of an electric-quadrupole moment or, alternatively, to the average value of the angular momentum tensor $3L_z^2-L^2$, often called the alignment. We chose to plot the density matrix elements rather than the second and third

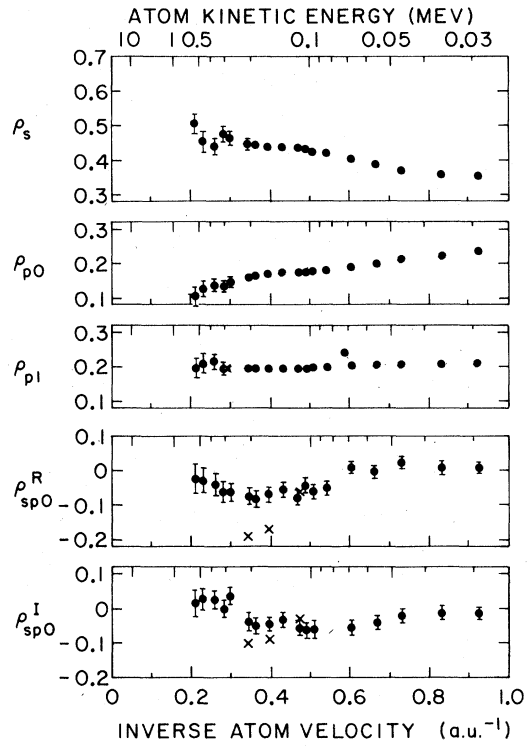

FIG. 3. The $n=2$ density matrix elements, normalized to unit probability for $n=2$ production, as functions of inverse velocity of the hydrogen atoms. Measurements from Ref. 8 are denoted by x.

observables when we discovered that ρ_{p1} is nearly independent of energy over the range we measured.

The complete measured $n=2$ density operator is plotted in Fig. 3 as a function of the inverse velocity of the hydrogen atom. We calibrate the abcissa in units of inverse velocity because molecular effects would depend upon the time spent near the foil surface and would thus be periodic in inverse velocity. The uncertainties in these points are primarily due to the nonlinear fitting procedure for ρ_s, ρ_{p0}, and ρ_{p1}. Numerical experiments suggest that the uncertainties are on the order of the dot size for all but the highest energy points. Here, uncertainties are several times larger because less periods of the Lamb-shift oscillation could be measured. The additional uncertainty introduced, because we used the alignment reported in Ref. 6 to determine ρ_{p0} and ρ_{p1} from the $\rho_{p0}+2\rho_{p1}$ we measured, is also of the order of the dot sizes. The uncertainties in both of the vector components are approximately twice as large because of the higher statistical uncertainties in the difference curves. The measurements of Ref. 8 are plotted as x.

In summary, the vector components ρ^R_{sp0} and ρ^I_{sp0} indicate that the bound electron leads the

proton and is moving faster, consistent with earlier measurements.[8] As mentioned earlier, ρ_{p_1} is nearly independent of energy over the measured range. Also notable is the increased relative probability of $2s$ excitation at the highest energies shown in Fig. 4.

The only model presently available for comparison with our measurements is the surface electric field model proposed by Eck[12] and extended by Lombardi.[13] As used by Lombardi, a strong surface field (10^8 V/cm) at the carbon target's exit surface mixes levels of atoms produced by the ion-target interaction. For this model to have any validity, these atoms must be formed well within the range of the surface field. Whether atom formation occurs this quickly is difficult to assess, since neither the electron capture process nor the source, range or time dependence of the surface field is known. It seems likely, however, that a field of 10^8 V cm would be closely related to the electron capture process.

Kupfer and Winter[14] recently applied the surface field model to alignment measurements. They distinguished between a time t_0 at which a neutral hydrogen atom is formed with $n = 2$ and a time t_1 at which this atom moves out of range of a surface electric field, a range they assume is a "few Bohr radii." They thus express $\rho_{p_0}(t_1)$ as a function of $\rho_{p_0}(t_0)$, $\rho_{s_0}(t_0)$, and $\rho^R_{sp_0}(t_0)$ and of a phase φ which is independent of energy. They note that ρ_{p_1} is conserved in the field region. They also seek to fit the measured alignment from Ref. 6 to the density matrix elements at t_0 (above).

At this point Kupfer and Winter seem to mistakenly assume that earlier time-resolved measurements provide information about the density matrix elements at t_0, thus tacitly assuming that it is experimentally possible to distinguish between t_0 and t_1. Correct use of the surface field model would therefore also include expressions for the measured $\rho_{s_0}(t_1)$ and $\rho^R_{sp_0}(t_1)$ in terms of the three t_0 elements above and the phase. Only ρ_{p_1} and $\rho^I_{sp_0}$ are conserved. The correctly applied field model is thus impossible to test by our measurement. At each energy three measured parameters $[\rho_s(t_1)$, $\rho_{p_0}(t_1)$, and $\rho^R_{sp_0}(t_1)]$ must be fit to three t_0 parameters $[\rho_s(t_0)$, $\rho_{p_0}(t_0)$, and $\rho^R_{sp_0}(t_0)]$ and to the energy-independent phase. At the 10^8 V cm mentioned in Ref. 14, mixing with $n = 3$ states is likely to complicate matters even more.

Partly in response to these theoretical difficulties, we present these measurements in the hope of stimulating theoretical work on this problem. We hope that refinements of a correct surface field model or some other approach will be able to account for the $n = 2$ density operator in this critical region where projectile and target electron velocities are nearly matched.

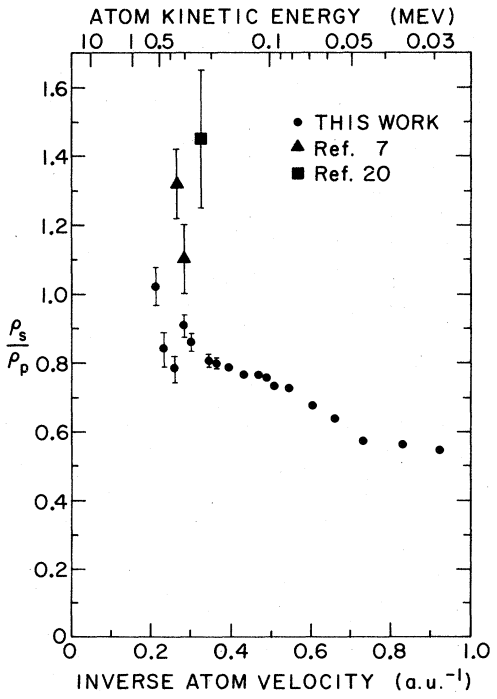

FIG. 4. The ratio of probabilities for excitation of $2s$ and $2p$ states.

V. THE PROBABILITY FOR THE EXCITATION OF $n = 2$ STATES

The density operator describes only the distribution of states within an average hydrogen atom produced by the beam-target interaction. In this section we report measurements of the probability that the beam-target interaction produces a neutral hydrogen atom with the density operator reported in the last section.

We obtained the $n = 2$ excitation probability from measurements of the absolute intensity of Ly α radiation corrected using the relative density operator of the last section. We used the apparatus described in Sec. II, except that we inserted a $\frac{1}{8}$-in.-diameter collimator, just upbeam ($\frac{1}{4}$ in.) from the $\frac{1}{4}$-in.-diameter foils, mounted to allow rotation in and out of the beam. We first measured the beam current at the carefully shielded Faraday cup, with no foil in the beam, using an Ortec beam current integrator. Next, we rotated a foil into the beam and measured the Ly α photon count rate. We converted the ratio of count rate to beam current into the total $n = 2$ excitation probability, plotted in Fig. 5 as a function of energy. The $n = 2$ excitation probability goes approximately as E^{-3}. This is to be compared with the amplitude

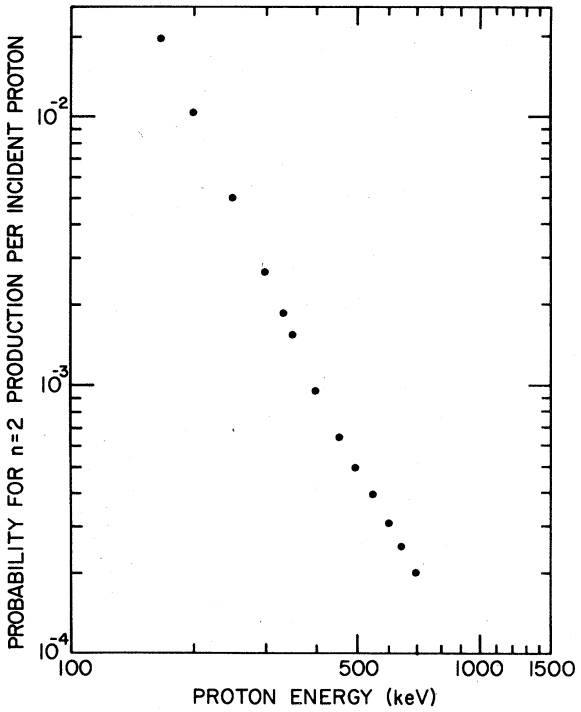

FIG. 5. The probability per incident proton for the production of $n=2$ states as a function of energy.

of the $n=3$ secondary electron cusp[3] and to charge-exchange cross sections,[18] both of which go as E^{-3}.

The absolute normalization, and hence the ordinate calibration provided for Fig. 5, is much less accurate than the relative normalization of the $n=2$ excitation probabilities at different energies. We assumed that the photomultiplier we used has a 5% quantum efficiency for Ly α radiation, as claimed by the manufacturer. As a result of tests made by varying the high voltage supplied to the photomultiplier and made by varying the amplifier settings, we estimate that we counted 95% of the pulses. These efficiencies, together with the detector solid angle we measured, determine the absolute intensity within an order of magnitude. Extrapolation of our measurements of the $n=2$ production probability to 1.2 MeV gives approximately 6×10^{-5}. This compares to the neutral hydrogen production probability of 2×10^{-4} measured by Gaillard *et al.*[15] at this energy.

VI. MOLECULAR EFFECTS

When H_2^+ and H_3^+ molecules break up within thin carbon targets, the protons from a single molecule remain correlated inside the target. The effect of this correlation upon the energy lost by each proton and upon its trajectory is well known in the Coulomb explosion literature.[4] Recently, Gaillard *et al.*[15] reported a study of the effects of such correlation upon the number of neutral hydrogen atoms produced per incident proton, as a function of the time spent by the protons within the target. In this section we report studies of $2p$ production made by measuring the Ly α radiation intensity per incident proton, as a function of target thickness. Our measurements permit a simple interpretation. From Ref. 15 we know that the dwell times used here are long enough to completely destroy correlations of the electrons incident with the proton cluster.

In Fig. 6 we plot the normalized Ly α intensity $I(t)/I(\infty)$ as a function of the time t spent by the proton cluster within the target. These different dwell times correspond to foils of thickness between 2.0 and 34 $\mu g\,cm^2$. We convert the thickness specified by the manufacturer in $\mu g\ cm^2$ to dwell time using the cluster velocity and assuming that the specific gravity of the carbon target is 1.65, as reported in Ref. 15. At the top of the figure we calibrate the abscissa in terms of the proton separation at the exit surface, calculated by using $r_0=1.08$ Å as the initial proton separation of H_2^+ [18] and $r_0=0.97$ Å as the initial proton separation of H_3^+,[19] assuming that an unscreened Coulomb repulsion occurs within the target. Uncertainties are equal to the triangle sizes.

The measurements plotted have several distinct

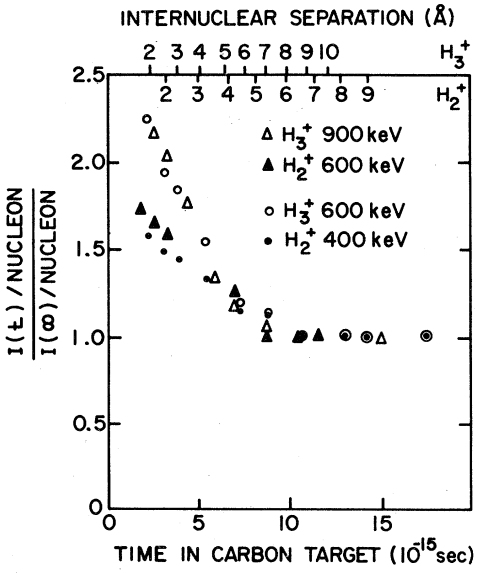

FIG. 6. Lyman α intensity as a function of dwell time, normalized to the long-dwell-time equilibrium value.

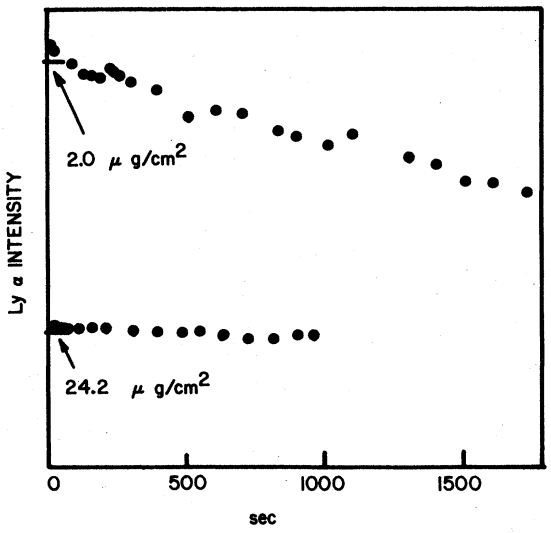

FIG. 7. Lyman α intensity as a function of time exposed to a 6.3 μA cm^2 H_3^+ beam. At $t = 0$ the carbon foils used to produce the upper and lower curves were 2.0 and 24.2 μg cm^2, respectively.

features. First, the intensity curves approach an equilibrium value, at dwell times which correspond to a proton separation of 6 Å at the exit surface of the target, for both H_2^+ and H_3^+ projectiles. Second, the approach to equilibrium seems to be linear in the dwell time. Third, an extrapolation to a dwell time of zero shows that the Ly α intensity (and hence the $2p$ production) per incident proton is roughly proportional to the number of protons simultaneously within the target. A simple explanation is that each proton leaves the foil accompanied by continuum electrons. The protons seem able to capture each others' continuum electrons up to a proton spacing of about 6 Å.

A related coherence phenomenon, first observed by Bickel,[20] seems also to be due to the proximity of protons which enter the target as part of the same molecule. When we measure the Ly α decay curves using incident H_2^+ and H_3^+ molecules instead of protons, we observe no interference beats at all for the thinnest carbon foils. We suggest that this occurs because the closely spaced protons interact strongly, thus dominating the mechanism which produces the orbital polarization discussed earlier in this paper. No net coherence is produced by the interaction of the closely spaced protons because the axis connecting them is randomly oriented in space. We observed that the interference beats returned when we used thicker targets.

Further measurement of this phenomenon, that is, of the $n = 2$ density-operator components as a function of energy and foil thickness for hydrogen atoms produced when H_2^+ and H_3^+ molecules are passed through thin carbon targets, would provide valuable information about the range of the foil-projectile interaction. The target thickness required to obtain the same density operator obtained with protons incident would correspond to a proton-proton separation such that the proton-proton interaction is negligible compared to the foil-projectile interaction. Unfortunately, at our vacuum of 3×10^{-6} Torr, the foils thicken appreciably during the time required to make a complete decay intensity measurement. We used the variation of the Ly α intensity as a function of dwell time (Fig. 6) to monitor the increase in target thickness as a function of time, as illustrated in Fig. 7. We began with a 2.0 μg cm^2 carbon foil (upper curve), sent a 6.3 μA cm^2-beam of H_3^+ through it, and monitored the Ly α radiation emitted downbeam from the target. The decrease in Ly α intensity corresponds to an increase in target thickness. There was no change in the Ly α intensity after the 24.2 μg cm^2 target (lower curve). We also found that the rate of thickening increases with increasing beam current density, consistent with the study of target thickening reported by Dumont, Livingston, Baudinet-Robinet, Weber, and Quaglia.[21] They and others[22] found that thickening can be effectively eliminated by placing a liquid nitrogen "cold finger" near the surfaces of the target.

ACKNOWLEDGMENTS

I am especially grateful to H. Gordon Berry for the support, encouragement, and suggestions which made this work possible. Several people helped with data acquisition, including A. E. Livingston, J. Stadelman, S. Huldt, T. Gay, R. DeSerio, and R. M. Schectman. Their help is gratefully acknowledged. I also thank H. Winter for providing alignment data before publication. I am grateful for personal support from a Danforth Fellowship and an Argonne Universities Association Graduate Fellowship during earlier and later stages of this work, respectively. This work was supported in part by the Department of Energy, Division of Basic Energy Sciences, and by a National Science Foundation Grant No. NSF PHY 81060.

*Submitted to the Department of Physics, The University of Chicago, in partial fulfillment of the requirements for the Ph. D. degree.

†Present address: Department of Physics, FM-15, University of Washington, Seattle, Washington 98195.

[1]H. G. Berry, Rep. Progr. Phys. 40, 155 (1977).

[2]H. Bukow, H. Buttlar, G. Heine, and M. Reinke, in *Beam Foil Spectroscopy*, edited by I. Sellin and D. Pegg (Plenum, New York, 1975), p. 263, H. Betz, Rev. Mod. Phys. 44, 465 (1972); L. Bridwell, J. Biggerstaff, G. Alton, C. Jones, P. Miller, Q. Kessel, and B. Wehring, in *Beam Foil Spectroscopy*, edited by I. Sellin and D. Pegg (Plenum, New York, 1975); B. Dynefors, I. Martinson, and E. Veje, *ibid.*, p. 231.

[3]M. Menendez and M. Duncan, in *Beam Foil Spectroscopy*, edited by I. Sellin and D. Pegg (Plenum, New York, 1975), p. 623; W. Meckbach, *ibid.*, p. 577; K. Groeneveld, *ibid.*, p. 593; M. Duncan and M. Menendez, Phys. Rev. A 13, 566 (1976).

[4]D. S. Gemmell, J. Remillieux, J. C. Poizat, M. J. Gaillard, R. E. Holland, and Z. Vager, Phys. Rev. Lett. 34, 1420 (1975).

[5]P. Dobberstein, H. Andrä, W. Wittmann, and H. Bukow, Z. Phys. 257, 272 (1972).

[6]H. Winter and H. Bukow, Z. Phys. 277, 27 (1976).

[7]M. Alguard and C. Drake, Phys. Rev. A 8, 27 (1973).

[8]A. Gaupp, H. Andrä, and J. Macek, Phys. Rev. Lett. 32, 268 (1974).

[9]I. Sellin, D. Moak, P. Griffin, and J. Biggerstaff, Phys. Rev. 31, 1335 (1973).

[10]T. Eck, Phys. Rev. Lett. 31, 270 (1973).

[11]G. Gabrielse, Phys. Rev. A 22, 138 (1980).

[12]T. Eck, Phys. Rev. Lett. 33, 1055 (1974).

[13]M. Lombardi, Phys. Rev. Lett. 35, 1172 (1975).

[14]E. Kupfer and H. Winter, Z. Phys. A 285, 3 (1977).

[15]M. J. Gaillard, J. C. Poizat, A. Ratkowski, J. Remillieux, and M. Auzas, Phys. Rev. A 16, 2323 (1977).

[16]M. Lombardi, M. Giroud, and J. Macek, Phys. Rev. A 11, 1114 (1975).

[17]H. Bukow, H. Buttlar, D. Haas, P. Heckmann, M. Holl, S. Schlagheck, D. Schürmann, R. Tielert, and R. Woodruff, Nucl. Instrum. Methods 110, 89 (1973).

[18]Z. Vager, D. S. Gemmell, and B. J. Zabransky, Phys. Rev. A 14, 638 (1976).

[19]M. Gaillard, D. Gemmell, G. Goldring, I. Levine, W. Pietsch, J. Poizat, A. Ratkowski, J. Remillieux, Z. Vager, and B. Zabransky, Phys. Rev. A 17, 1797 (1978).

[20]W. Bickel, Phys. Rev. A 12, 1801 (1975); J. Opt. Soc. Am. 58, 213 (1967).

[21]P. Dumont, A. Livingston, Y. Baudinet-Robinet, G. Weber, and L. Quaglia, Phys. Scr. 13, 122 (1976).

[22]D. Gemmell (private communication).